I HEREBY STATE THAT

this thesis entitled

Use of SOLIS *Satellite-based Solar Spectral Irradiance for Characterization of Thin Film Photovoltaic Modules*

is the result of my work, using only the quoted resources.

Diego Alejandro Sanchez Herrera

Augsburg, Germany

July 18 2007

Table of Contents

List of Figures

List of Tables

Abstract

The aim of this thesis is the outdoor characterization of *PV* modules using spectral irradiance data. This data is calculated on the basis of the coupling of satellite meteorological information with a radiative transfer model. Measurements of the characteristic curves of a poly-crystalline Silicon *c-Si* and an amorphous Silicon module *a-Si* are performed on horizontal surface. A third intermediate technology *CdTe* is characterized theoretically. Measurements of global broad band irradiance are performed also on horizontal surface. The characterization of the modules is based on the modeling of the short circuit current I_{sc} as function global broad band irradiance and the inclusion of spectral parameters.

For spectral analysis we have at hand two spectral parameters in the form of positive real numbers: The *Average Photon Energy APE* and the *Used Fraction UD*. The first parameter is a pure descriptor of the spectral variations of the spectrum of the Sun, while the second considers the influence of the spectral fluctuations coupled to the spectral response of the *PV* device under investigation. The APE parameter is calculated only with the satellite-based spectral irradiance, while UD requires the spectral irradiance and the spectral response of the *PV* device. Another parameter, which resulted particularly useful for understanding the previous parameters is the *Clear Sky Index* k^* calculated from the satellite based *Cloud Index n*.

In this first attempt to use satellite-based irradiance for modeling short circuit current, many relevant aspects were investigated, which will help to define future approaches to model *PV* devices, not only in the cases of using irradiance data based on satellite information.

Acknowledgements

I want to express my gratitude to several persons who collaborated in the completion of this thesis:

To *Meteocontrol GmbH* for supporting this research project, especially to Dipl. Ing. (FH) Stefan Bofinger. In Oldenburg University to Dr. Elke Lorenz for her devoted assistance and fruitful discussions; equally to Dr. Annette Hammer. Also to my colleague MSc. Mauricio Rojas and Dipl. Phys. Udo Kulchewski for their willingness to discuss basic aspects of this work. To *First Solar GmbH* for kindly providing the *CdTe* modules.

Chapter 1

Introduction

The efficiency of *photovoltaic (PV)* modules changes depending on the operating conditions. Therefore it is worth to dedicate efforts to understanding at what extent and how these variations occur.

Many factors alter the operation of the *PV* devices: Irradiance, temperature of the device, angle of incidence, Air Mass, cloud conditions and ratio of diffuse and direct irradiance. In this work we will concentrate on the effects on the short circuit current values, because this parameter is the one related to power production which results mostly affected by varying operating conditions. Differently, the voltage is much more stable.

Up to now the effects of irradiance and temperature have been considered as the most significant. The well known linear model between broad band irradiance and short circuit current is used nowadays, as well as the model describing fractional variations on the short circuit current value for varying temperatures. However these models are beginning to be insufficient for emerging technologies and for the growing need of confidence in the design of power plants. This need has its origin in the need for satisfying the everyday growing demand for energy [*], which drives advances

[*]The focus of this work is pure technical; however the social-economical context is relevant and I am convinced that we should not only look for more and cleaner ways to obtain the energy, but reconsider why so much energy is being required. A significant reduction of the energy demand worldwide can only occur under rational use of the resources, which is interlinked with a change in the habits of living and production. These changes are only possible if the present economical models make room for them.

in different fields of natural sciences. In this way the so-called *Thin Film* technologies land in our discussion: Briefly this is a *PV* technology developed in the last two decades, which differs in four main aspects from the traditional Silicon crystalline technologies [7]:

1. Thin and long cells with high rate of photon-electron conversion. The cells are about $1\mu m - 6\mu m$ thick, while *c-Si* cells are about $200\mu m - 300\mu m$.
2. Low consumption of material per peak power unit produced: $0.2kg/kW_p$ vs $16kg/kWp$.
3. Lower consumption of primary energy per peak power unit: $5MWh/kW_p$ vs $14MWh/kWp$.
4. *Better* performance under low irradiance conditions and high diffuse fractions.

The points two, three and four in our list of advantages talk about potential economical benefits of using *thin film* technologies. Points two and three are related to the *module's production side* while point four is related to the *module's energy yield side*. However what could look like a double-sided gain, may or may not be like that: *Thin film* devices are *normally*[†] less efficient than crystalline Silicon devices; however they may be cheaper to produce. So it seems we have a reduction of costs in one side and a reduction of the energy yield in the other. The question is whether the overall balance will be better, worse or equal than the one of the crystalline technologies when spectral considerations are made.

Besides the costs of production, the prices of *PV* modules are determined by their *STC* performance values. However these conditions are extremely seldom found outdoors. On the other side of the economical balance, the energy yield depends on the *real life* conditions. Therefore a *PV* device with a superior *Performance Ratio (PR)* and lower costs of production looks like a promising technology. According to point four it may happen that this is the case for *thin film* technologies under cloudy and low irradiance conditions. This is what we would like to find out. A long way is ahead before getting there: We have basic new stuff included: Spectral irradiance data modeled

[†]Under *Standard Test Conditions:* $1000W/m^2$, $25°C$ cell temperature, $AM1.5G$

from satellite information coupled with ground measurements. Many other targets will appear in between, related to the recognition of the possibilities of this scheme of spectral characterization.

The experiences characterizing *thin film* technologies with the variables global broad band irradiance and temperature have suggested that something is missing in the analysis (due to poorer results). Examples of *PV* modules characterizations can be found in [11] [10] [8] [9]. A pioneer work using ground measured spectral irradiance has been performed by T.R. Betts [2] at *Loughborough University* in the *UK* in recent years (2004). This work constitutes a reference for the present research.

Along this document we will get a comprehensive view of the work performed. We will start in **chapter 2** with a brief introduction to the scheme *satellite - radiative transfer model (SOLIS)* used for the calculation of the spectral irradiance. In **chapter 3** we will know about the ground measurements and the technical details of the *PV* modules used in the research. In the **chapter 4** the spectral parameters used in this work will be introduced and analyzed by using *SOLIS* irradiance data. In this chapter the short circuit current spectral models will be proposed. In **chapter 5** we will analyze how the spectral variations manifest in the data and how the use of ground measured data together with *SOLIS* data interferes with the observation of the spectral effects. Finally the proposed spectral models will be applied. In the last chapter the relevant conclusions will be summarized together with suggestions for further analysis of spectral effects on *PV* devices.

Chapter 2

The Satellite-based Spectral Data: *SOLIS*

SOLIS is an acronym for ***SO****lar* ***I****rradiance* ***S****cheme*. It is a method for the calculation of the solar irradiance on Earth's surface (on horizontal plane) based on satellite images with cloud information and data containing information about the aerosols, water vapor and ozone of the atmosphere. *SOLIS* has the capability to resolve spectral irradiance in 26 bands and its output is available in hourly values and slot values (every fifteen minutes) for a location on Earth specified by latitude, longitude and altitude above mean sea level.

SOLIS works through the linkage of two modules: the clear sky module and the cloud module.

2.1 The Clear Sky Module

The calculation of the irradiance for defined regions on Earth's surface is made with information from the following satellites:

MSG-2 O_3, water vapor

ERS-2/ENVISAT Aerosols, O_3

This information allows the calculation of the irradiance in W/m^2 for a given time on a given place on Earth in 26 wavelength bands starting at 306.8 nm and ending at 3001.9 nm [13]. The broadband irradiance corresponds to the sum of the values of the 26 bands.

The clear sky module uses as special feature the combination of a radiative transfer model (*RTM*) and a fitting function called the *Modified Lambert-Beer* function (*MLB*). The spatial coverage requirements of the *SOLIS* scheme require that all the calculations are performed on short times. However using the *RTM* for all the calculations would take too long. This is the reason why the *RTM* is used only a few times per day for the determination of the *MLB* functions for irradiance. The way in which the clear sky module works is depicted in the following paragraphs.

The simple relationship that describes the attenuation of monochromatic light by matter of attenuation coefficient or optical depth τ is given in equation 2.1.

$$I = I_0 \cdot \mathrm{e}^{-\tau} \tag{2.1}$$

In our case, the irradiance is evidently dependent on the hour of the day, it is, on the solar zenith angle of the sun (*SZA*). A modified expression taking into account this fact is equation 2.2, in which a modified optical depth varying with *SZA* and a multiplicative factor also dependent on *SZA* are implemented.

$$I(\theta_z) = I_0 \cdot e^{(-\tau/\cos\theta_z)} \cdot \cos\theta_z \tag{2.2}$$

The corresponding equation for polychromatic light corresponds to equation 2.3; this is the so called *Modified Lambert-Beer* function (*MLB*) and can be found in [14]. τ_0 is the optical depth at *SZA* of 0° and a is a correction parameter calculated at a *SZA* of 60°. This equation is the fundament of the calculation of the clear sky irradiance in polychromatic bands and broad band and holds for

direct and diffuse components (therefore also for global irradiance). The a parameter accounts for the polychromatic character of the light and is necessary due to the non-additivity of the attenuation coefficients τ for monochromatic light. The values of this parameter differ for each case: direct, diffuse and global components. It should be noted that the *MLB* is a fitting function although its roots are in the well known exponential attenuation of radiation by matter.

$$I = I_0 \cdot e^{(-\tau_0/\cos^a(\theta_z))} \cdot \cos\theta_z \tag{2.3}$$

This means that after calculation of τ_0 and a, a function for the calculation of clear sky irradiance on Earth's surface for any time of the day is available. This means that the radiative transfer model will be only used twice (0° and 60° *SZA*) for one day and the the rest of the values will be calculated using the *MLB* relationship. Notice that with τ_0 and a fixed, the *MLB* is only a function of *SZA*. In figure 2.1 plots of solar irradiance curves calculated with the *MLB* function are displayed and compared to several points obtained with the *RTM*. The spatial resolution of the clear sky data is $50km$ x $50km$.

2.1.1 The Radiative Transfer Model: *libRadtran*

The *RTM* used is called *libRadtran* and consists in a library of *C* and *FORTRAN* code for the calculation of solar radiation in the Earth's atmosphere. This model considers not only the turbidity of the atmosphere but the aerosol composition separated from the water vapor. This is a requirement for the reliability of the spectral distribution of the irradiance. The *libRadtran RTM* is compatible with the *Kato spectral bands*, the ones selected for *SOLIS*. For more information on this model please refer to [14] and [1].

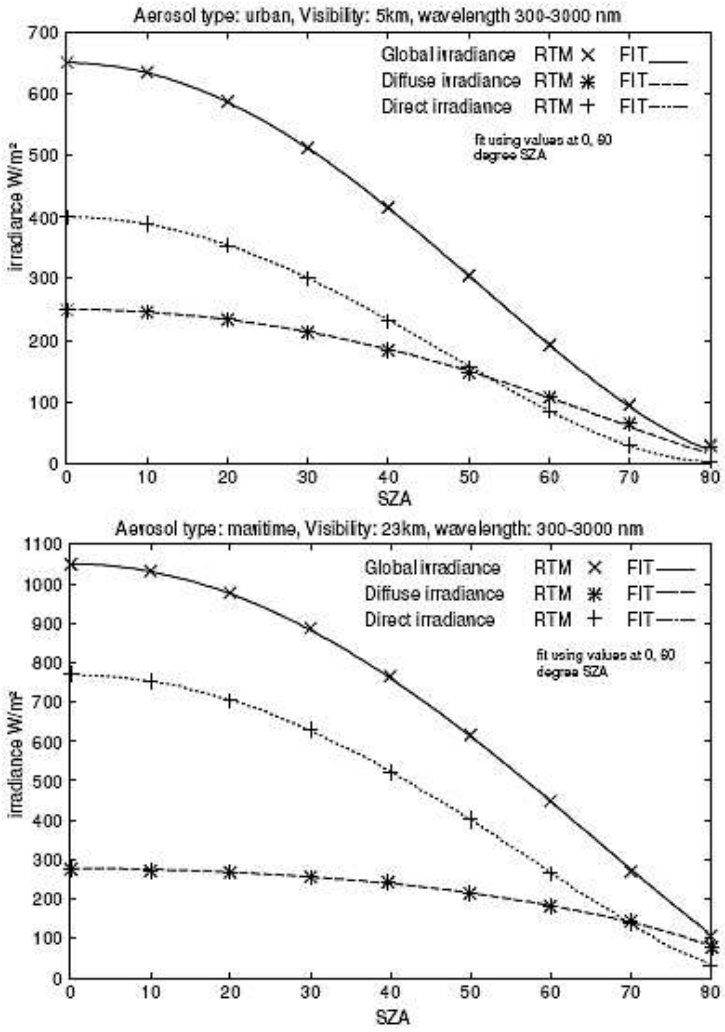

Figure 2.1: Comparison of solar irradiance calculations as function of SZA based only on RTM and based on RTM and MLB for two different atmospheric clear sky conditions [14].

2.2 The Cloud Module

The cloud module completes the solar irradiance scheme and calculates the irradiance on Earth' surface according to equation 2.4. In this equation k^* is the *Clear Sky Index*, whose values are calculated from the *Cloud Index* values n. The values of clear sky irradiance are obtained from the Clear Sky module.

$$G = k^* \cdot G_{ClearSky} \tag{2.4}$$

The cloud module works based on the cloud information supplied by the satellite *MSG-2*; with a temporal resolution of 15 minutes and a spatial one of $1km$ x $1km$. The n values are derived from normalized cloud reflectivity and the k^* values are calculated from the n-k^* relationship (see equation 2.5).

$$k^* = \begin{cases} 1.2 & n \leq 0.2 \\ 1 - n & 0.2 < n \leq 0.8 \\ 1.6667n^2 - 3.6667n + 2.0667 & 0.8 < n \leq 1.1 \\ 0.05 & n > 1.1 \end{cases} \tag{2.5}$$

2.3 The Quality of the Data

Validation of the *SOLIS* data is only available for broad band irradiance. The errors depend on the location, the time of the year and the time scale of the data (hourly, monthly values, etc). In general it has been observed that the absolute error in the calculation of global broad band irradiance is higher for summer than for winter. On the other hand the relative error is higher in winter (30%-40%) than in summer (15%-25%) due to lower values of irradiance. An example on the variation with the time scale for a location in Germany in summer supply the following values:

- 1min: rmse=35%

- 5min: rmse=32%
- 10min: rmse=28%
- 30min: rmse=22%
- 60min: rmse=19.5%

For more information about the errors of the *SOLIS* broad band irradiance data please refer to [12].

Validation of the *SOLIS* spectral data with ground measurements of spectral irradiance is not available yet, but it is expected that it will be performed soon.

Chapter 3

Photovoltaic Modules Used and the I_{SC} Measurements

In this chapter the technical description of the *PV* modules under investigation is given. Also relevant information concerning the ground measurements of short circuit current and global broad band irradiance.

3.1 The Photovoltaic Modules

Three types of *PV* modules have been used in this work. The reference technology is a poly-crystalline module and the *thin film* technologies are represented by amorphous Silicon and Cadmium-Telluride modules. In total we have 9 modules distributed like this:

1. Two already used *a-Si* modules *Tianjin- Jinneng*.
2. Four brand new *CdTe FS-62* modules provided by *First Solar*.
3. One used poly-crystalline module *Hyundai HiS-M188SF*.

Module Type	*a-Si*	*c-Si*	*CdTe*
P_{MPP} $[W]$	38±1	188±4%	62.5±3.1
V_{MPP} $[V]$	45	26.2	64
I_{MPP} $[A]$	0.84	7.20	0.95
V_{OC} $[V]$	60	33.0	91
I_{SC} $[A]$	1	7.87	1.14
P_{MPP} T coefficient	-	-0.32%/°C	-0.25%/°C
V_{OC} T coefficient	-0.28%/°C	-0.30%/°C	-0.29%/°C
I_{SC} T coefficient	+0.09%/°C	+0.08%/°C	+0.04%/°C
Cell type	*a-Si*	6" *poly c-Si*	*CdTe*
Number of cells		54	116
Cell efficiency [%]	-	14.3	-
Module efficiency [%]	-	13.0	-

Table 3.1: Electro-technical data of the PV-modules used in the experiment. The data is supplied for one module at *STC* conditions ($1000W/m^2$, $AM1.5G$ and module temperature of 25°C).

The electro-technical data of these modules are presented in table 3.1.

The spectral response curves of the devices were sampled and average values were calculated according to the wavelength bands used by *SOLIS* for delivery of the spectral irradiance data.

3.1.1 *a-Si Tianjin Jinneng*

For the measurements the two modules available were connected in parallel in order to increase the current output.

The spectral response curve for this model was not found, so we took a curve from [18]. This is an early study on the spectral effects on the power production of photovoltaic modules carried out at the *Fraunhofer Institut fuer Solar Energiesysteme (ISE)* in Freiburg, Germany. See Fig. 3.1 on page 13.

3.1.2 *CdTe First Solar FS-62*

These four brand new modules were kindly provided by *First Solar GmbH*. Two of them were used in parallel to increase the current output. The other two were kept under dark conditions in order to

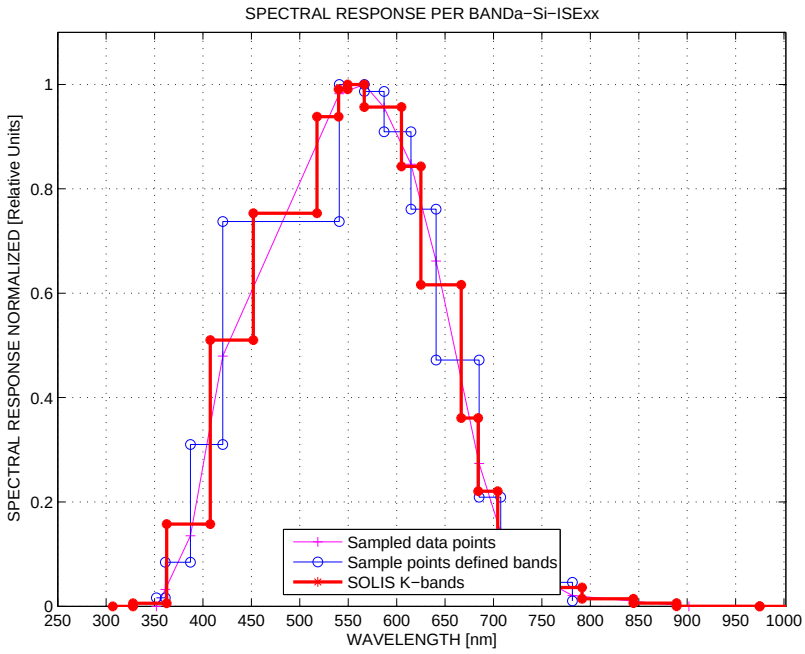

Figure 3.1: Spectral response assumed for *a-Si*. Three curves are displayed: 1. The sampled curve. 2.The mean values for the bands defined by the sampled points. 3.The mean spectral response for the *SOLIS Kato-bands*. This last curve will be used for the calculation of *device-dependent* spectral parameters. Taken from [18].

be able to perform a later comparison of the effects of the semiconductor degradation process that takes place in thin film modules during the first months of operation.

Each module is ($1200mmx600mmx6.8mm$) with a mass of $11.4kg$ and has 116 *CdTe* cells. These modules are of the type *frameless laminate*.

For these modules, the manufacturer supplied a quantum efficiency curve which was taken as the spectral response of the modules [5] (See Fig. 3.2 on page 15). Taking the quantum efficiency as the spectral response implies an error because the amount by which both quantities differ depends on the inverse of the wavelength of the light considered. This can be seen in equation 3.1 on page 14. Here EQE_{λ_0} is the *External Quantum Efficiency* of the device at a fixed wavelength λ_0 in $A/(photon/s)$ or $electron/photon$; i.e. the electrical current output divided by the photon flux ϕ_{λ_0}. SR_{λ_0} is the corresponding spectral response in A/W.

$$
\begin{aligned}
&EQE_{\lambda_0} = \frac{\text{measured.current}}{\text{photon.flux}} = \frac{I_{\lambda_0}}{\phi_{\lambda_0}} \\
&\text{and} \\
&SR_{\lambda_0} = \frac{\text{measured.current}}{\text{incident.power}} = \frac{I_{\lambda_0}}{P_{\lambda_0}} \\
&\text{because} \\
&\phi_{\lambda_0} = \frac{\lambda_0 P_{\lambda_0}}{hc} \\
&\text{follows :} \\
&EQE_{\lambda_0} = hc\frac{SR_{\lambda_0}}{\lambda_0}
\end{aligned}
\tag{3.1}
$$

Because we are interested in the relative spectral responses, the magnitude of this error for a fixed wavelength (which is in the order of *lambda*) is not important. What account for errors in our calculations is the artificial scaling introduced for different wavelengths. In equation 3.2 we have an explicit expression for the ratio of the spectral response values at two wavelengths as function of the ratio of the corresponding quantum efficiency values. This expression let us see that as the wavelength difference increase, the error introduced increases. In the case of *CdTe* the most significant case would be to calculate the error at about 500*nm* and 850*nm*. In this case we have that the ratio of spectral responses is about 1.7 times the ratio of quantum efficiencies. This means that the the shape of the EQE and SR curves differ: the latest has its maximum about 850*nm* while the first at about 500*nm*.

Despite taking the quantum efficiency curve as the spectral response curve is a childish error, it was detected at a later phase of the work and therefore **the results displayed for *CdTe* in this document have not been corrected.** This does not mean actually that the calculations for $CdTe$ are wrong, but can not be interpreted in the same fashion as the results for *a-Si* and *c-Si*. This is the case for the parameter UD introduced in chapter 4 which depend on the spectral response of the device.

$$
\frac{SR_{\lambda_2}}{SR_{\lambda_1}} = \frac{EQE_{\lambda_2}}{EQE_{\lambda_1}}\frac{\lambda_2}{\lambda_1} \tag{3.2}
$$

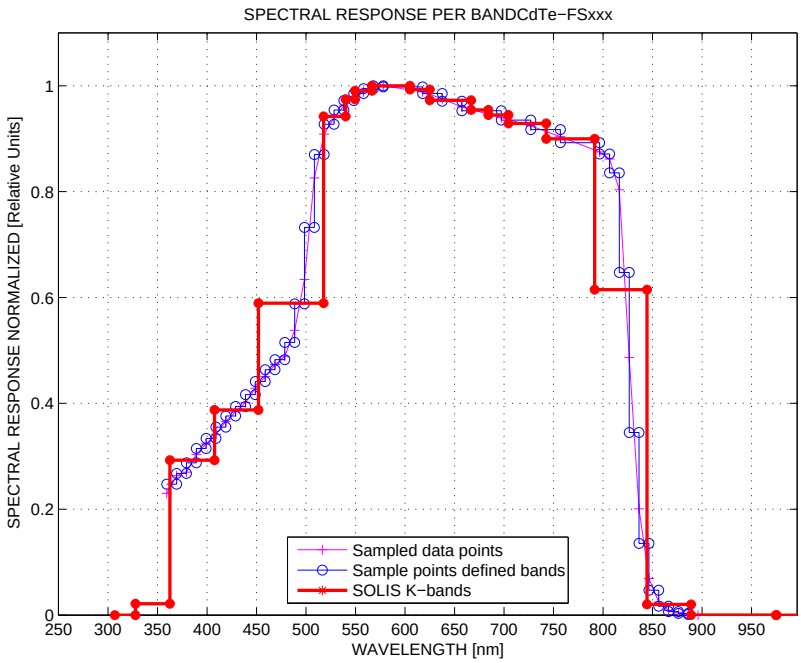

Figure 3.2: Spectral response of the *CdTe* modules. The curve was obtained from the producer as a quantum efficiency curve. Three curves are displayed: 1. The sampled curve. 2.The mean values for the bands defined by the sampled points. 3.The mean spectral response for the *SOLIS Kato-bands*. This last curve will be used for the calculation of *device-dependent* spectral parameters. Taken from [5].

3.1.3 *c-Si Hyundai HiS-M188SF*

This is the reference module. For crystalline photovoltaic technologies the influence of different light spectra is expected to be very low. In the experiment we used a single module given that the current output is high enough for a proper measurement. The module has 56 cells connected in series in a matrix of $9cells \times 6cells$. Its dimensions are ($1476mmx983mmx35mm$) and its weight is around $17kg$.

For this module the actual spectral response could not be found, so we used a curve from [4]. See Fig. 3.3 on page 16.

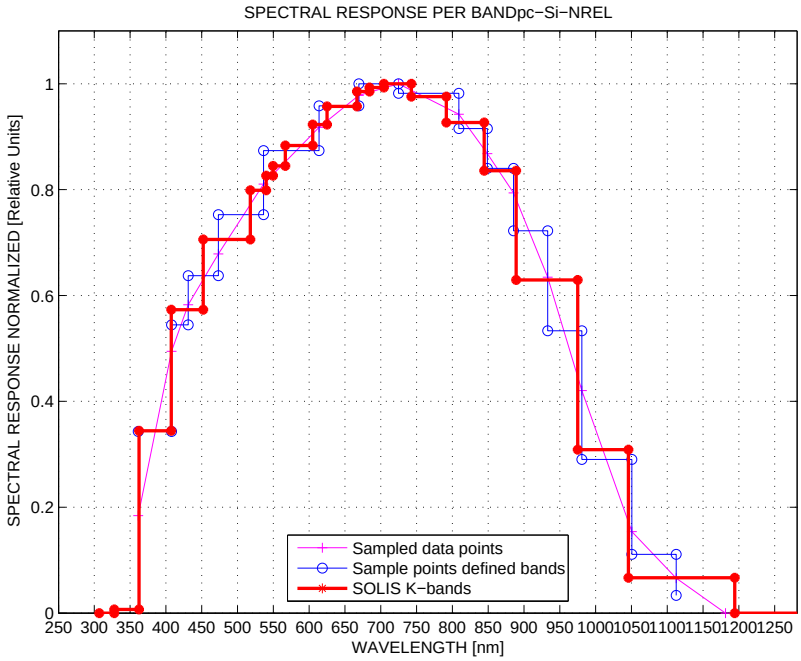

Figure 3.3: Spectral response assumed for the *c-Si* module. Three curves are displayed: 1. The sampled curve. 2.The mean values for the bands defined by the sampled points. 3.The mean spectral response for the *SOLIS Kato-bands*. This last curve will be used for the calculation of *device-dependent* spectral parameters. Taken from [4].

3.2 The Ground Measurements

The measurements of short circuit current and other parameters were performed with the device *PVPM-1000C* [15]. This device includes a *combi sensor* which consists in an irradiance sensor and a temperature sensor. A mono-crystalline Silicon cell measures the irradiance and the temperature on this cell is measured by a *PT-1000* sensor. It is easy to see that these measurements have 2 drawbacks:

1. The irradiance value is measured with the same type of device whose behaviour is to be investigated. This means that its readings will contain spectral effects.

2. We don't know how precise it is to assume that the temperature of the modules is equal to the measured temperature of the sensor cell. Even more, possibly the temperature of the modules

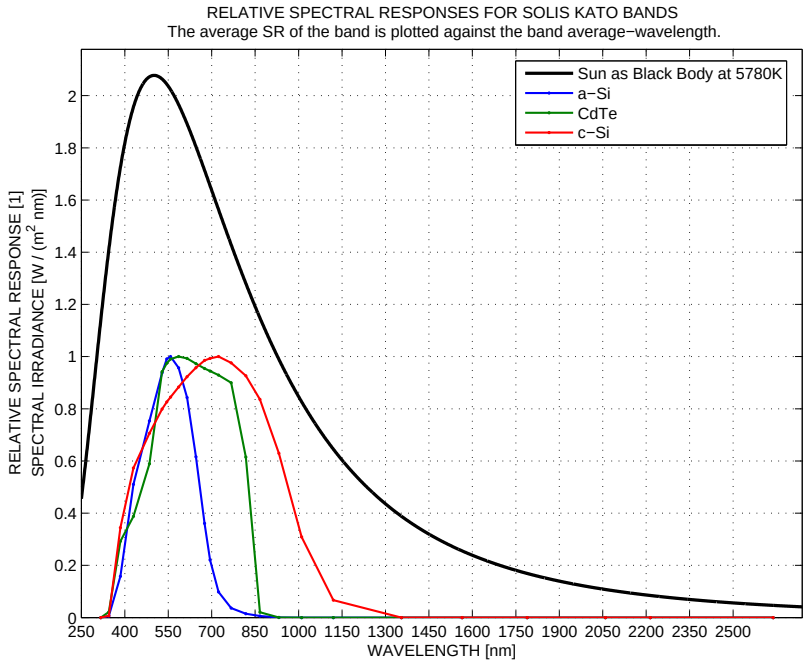

Figure 3.4: Relative spectral responses for the 3 modules under investigation and spectral irradiance for a *black body* at $5780K$ at the distance Sun-Earth from the Sun. The average values of the spectral responses have been plotted against the wavelength average value of each *SOLIS Kato-band*.

cannot be defined with the measurement of temperature at a single point. In the measurement setup The modules were set in such a way that air can easily flow below them for cooling purposes. Likewise for the sensor cell which is enclosed in a plastic box.

Every measurement of this device consists in the calculation of the characteristic curve of the module under the irradiance and temperature conditions at the moment. In this way a list of parameters is obtained after each measurement, which lasts about 2 seconds. The most relevant parameters are:

1. Global broad band Irradiance G $[W/m^2]$
2. Cell temperature T $[°C]$
3. Open circuit voltage U_{oc} $[V]$
4. Short Circuit Current I_{sc} $[A]$

Figure 3.5: Picture of the measurement setup. When the picture was taken (December 7 2006) the 2 $CdTe$ modules and the *c-Si* module were mounted. The *combi sensor* is in the lower-left corner of the picture. The rest of solar modules with no-null inclination have nothing to do with this research and are part of a grid connected power plant.

All the measurements were performed on horizontal surface.

Because most of the time we had only one measurement device, we had to alternate the measurements for the different modules. After measuring a few weeks the 3 module types, we decided to measure only for *a-Si* and *c-Si* given that in the group, they are the modules with the biggest difference in the spectral responses. In this way we *sacrificed* the only module for which we had a spectral response supplied by the manufacturer but gained more measurements for the chosen technologies under similar conditions. In general measurements were performed for one week for a module type and then we changed to the other.

3.2.1 Temperature Effects on the I_{sc} and G Measurements

Unfortunately much of the collected data had to be rejected for analysis because of problems which are or seem to be related to the temperature measurements. In the first place, in the last week of year

Figure 3.6: A characteristic curve measurement was carried out every 5 minutes and the data was stored in a *PC* connected to the measurement device. In May 2007 data was measured simultaneously with two similar measurement devices for *a-Si* and *c-Si*.

2006, it seems that a short circuit occurred in the sensor. All the temperatures registered for one week correspond to the lower limit of the sensed range of sensor, i.e. $-50°C$. After that we started to have problems with the measurement device: The continuous measurements were interrupted automatically after a few hours. The measurement device was sent for reparation and calibration twice, which stopped the measurements for about two months altogether. As the measurements were restarted on the abnormal hot and sunny days of April 2007, the data points for clear sky conditions displayed a strange behaviour which has not been understood completely but is related to temperature. This behaviour was observed for measurements of both module types *a-Si* and *c-Si* and is not recognizable with *SOLIS* irradiance. An example of this phenomenon is found in figure Fig. 3.8 on page 22. In this plot the data points for clear sky conditions are branched and form something similar to an ellipse. The upper branch corresponds to the *before noon* points and the lower branch to the *afternoon* data. In the afternoon the temperature values for a fixed irradiance value are higher than in the morning and nearly all the points are above $25°C$. In the morning not all the points are above this reference temperature, just the points above about $300W/m^2$. Because this

Figure 3.7: The Sun's path in the sky was calculated according to the geographical coordinates of the site. In this way the Sun elevation *horizon line* was calculated and the data points under this angle were ignored in the modeling analysis.

phenomenon occurs in the plots of *temperature corrected* and *non-corrected* short circuit current*, it seems that what we observe is an overestimation of the irradiance values. This overestimation may be due to two different reasons related to temperature:

1. The temperature coefficient used by the measuring device for calculating the *temperature corrected* values of global broad band irradiance seem to be underestimated. By checking the calibration of the device, a value of $5.8 \times 10^{-4}/°C$ was estimated.

2. Differences between the temperature of the sensor cell and the actual temperature of the modules. In this case it would mean that the temperature of the sensor is higher than the one of the modules. A look to the wind data of a meteorological station nearby may help to see whether this hypothesis makes sense or not.

3.2.2 Other Considerations about the Measurements

In Fig. 3.7 on page 20 we have a panoramic picture of the site of the measurements in Augsburg, in southern Germany. In this picture lines are drawn with the path of the Sun for different months of the year. The program used for that allows also the calculation of horizon line of the site, it is the Sun elevation angle above which no shadows due to surrounding objects exist. For most of the azimuthal directions, this value is 5°, however on the west side a building rises the horizon line to 12° for the azimuth angles in the range $265° - 280°$ †. These horizon line values are used for filtering the data by Sun elevation values, which are calculated according to the norm *DIN 5034*.

*For an explanation about the temperature model applied to short circuit current data, please refer to chapter 5 on page 59.

†The azimuth angle is 0° on the north, 90° in the East and 270° on the west.

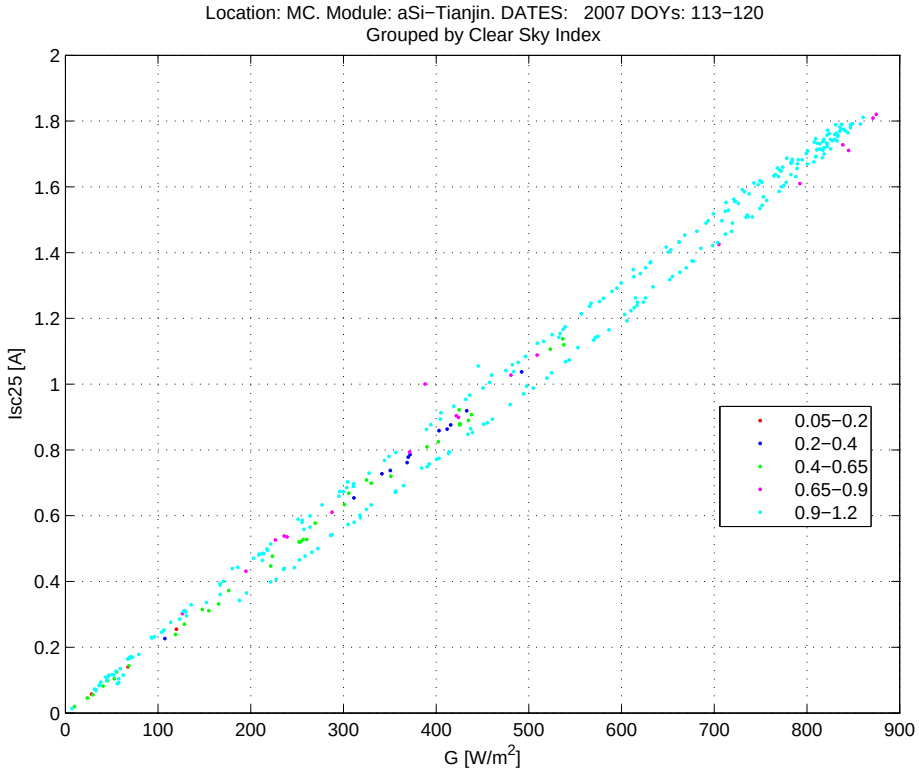

Figure 3.8: For the data of the sunny and hot days of April 2007 the short circuit current data points for clear sky conditions (pale blue points) split in two branches which form something similar to an ellipse. Although this phenomenon is not completely understood, it is related to high temperatures of the *PV* modules and the sensor cell.

Chapter 4

The Spectral Parameters *SPARs*

Firstly I want to introduce the acronym *SPAR* or *SPARs* (plural) for referencing the *SPectral PAramaeters*. They will save some valuable bits in the hard disk and a few microseconds in your brain when going through this document.

Let's recall the aim of this work: Modeling the I_{sc} production of photovoltaic modules taking into account the spectral variations of the solar irradiance. For this purpose we have at hand 2 spectral parameters: The APE or *Average Photon Energy* and the *Used Fraction* or UD. Both parameters have been already used in research works about spectral influences on PV devices (see [2] and [3]) and the present work is somehow a continuation of them. That is the reason why these two spectral parameters have been taken as starting points for our spectral analysis.

$$SPARs \begin{cases} APE \\ UD \end{cases} \tag{4.1}$$

It is important to realize at this point that when we talk about spectral parameters we have 2 different features which such parameters can describe:

1. *Chromatic* content: This is the distribution of the energy in the spectrum without regard of the magnitude of the spectral irradiance. We will be talking about *blue* and *red* spectra although the extraterrestrial and $AM1.5$ spectra have already a high blue (*UV-VIS*) content. Thus the blue spectra look similar to these reference ones, with a maximum about $500nm$; while the red ones are flatter with maxima shifted to higher wavelengths.

2. *Intensity*: The absolute amount of energy we get for each wavelength or frequency value. The integration of these energies will give the total energy "carried" by the given spectrum.

We will encounter these features frequently in the future and they will be keys for the understanding of this work. Before further explaining the parameters it may be helpful to review some features and facts about the solar spectrum itself (especially if you have not understood well the features a spectral parameter can describe or you don't know which are those *reference* spectra). Please refer to the appendix A. Likewise it will be useful to have some basic information about the data used for the analysis of the spectral parameters presented in the current chapter. This you will find in the coming section.

4.1 The Data Used for the *SPARs* Analysis

The data used for the analysis presented in this chapter are exclusively *SOLIS* satellite-based data. The data correspond to following dates of the year 2006:

1. Day of year (DOY): 152-214. June 1 - August 02.

2. Day of year (DOY): 280-324. October 7 - November 20.

3. Day of year (DOY): 331-365. November 27 - December 31.

In Fig. 4.1 the global broad band irradiance read directly from the broad band data files from *SOLIS* is compared to the integration (sum) of the global spectral irradiance read from the spectral data files

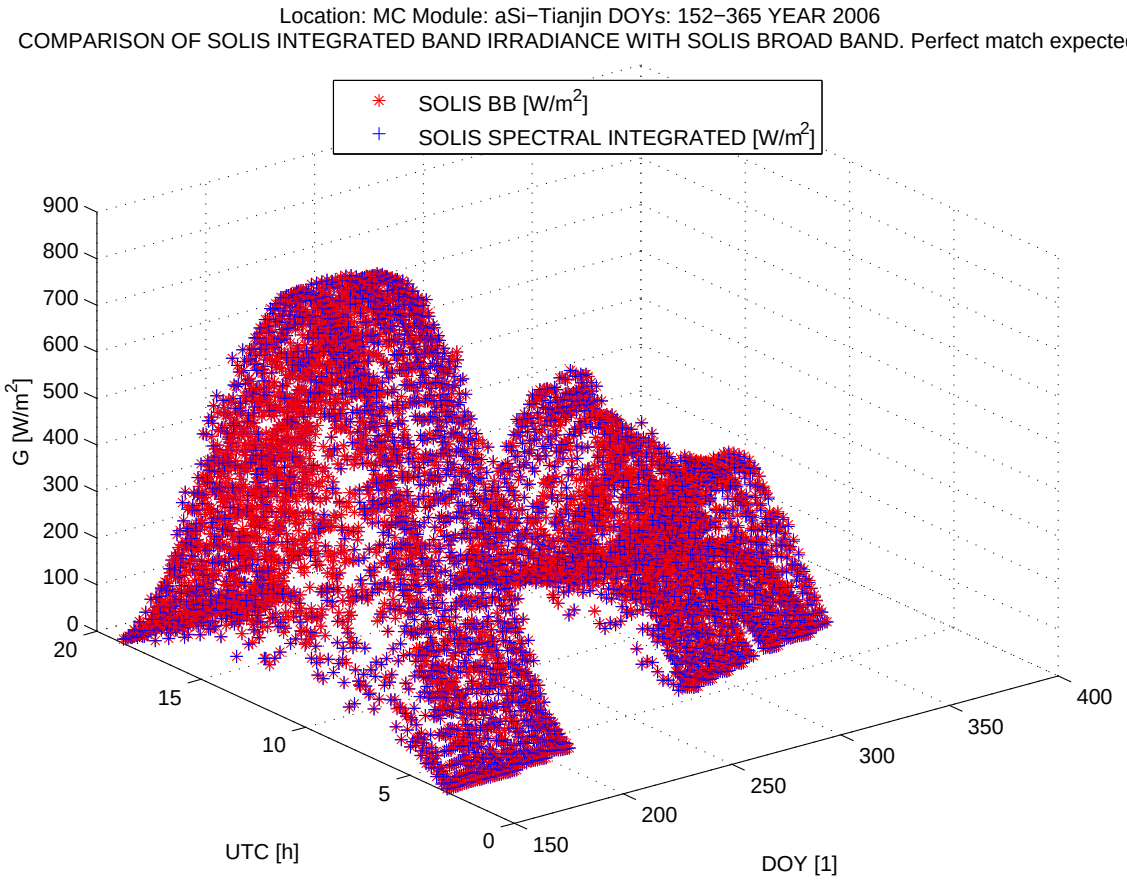

Figure 4.1: Time series of integrated spectral global irradiance and broad band irradiance

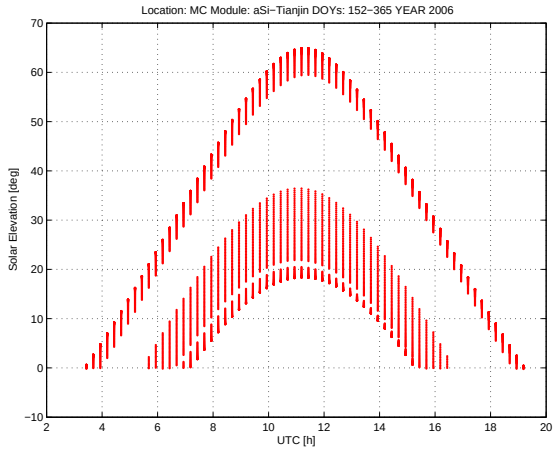

Figure 4.2: Solar Elevation γ_s vs UTC displaying seasonal variations.

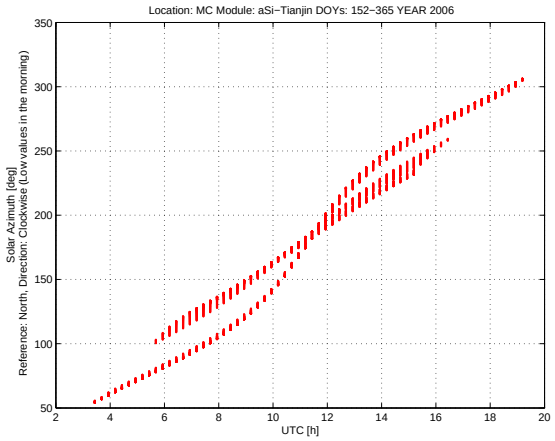

Figure 4.3: Solar Azimuth φ_s vs UTC displaying seasonal variations.

from *SOLIS*. For most of the cases both values match, however it is clear that for irradiances under about $300 W/m^2$ small discrepancies are frequent. It happened sometimes that the global spectral irradiance value of the 25^{th} *SOLIS* band contained *NaN* values. This however does not represent a big problem because the values of this band contribute a very low fraction of the total irradiance. For further plots and calculations the global broad band irradiances from the broad band *SOLIS* files are used.

In Fig. 4.2 and Fig. 4.3 the Sun elevation γ_s and Sun Azimuth φ_s are plotted against *UTC*.* The Sun coordinates were calculated according to the norm *DIN 5034* [16]. In these plots the seasonal variations can be recognized: Both angles reach the highest values in summer and have a wider range in the *UTC* axis. The reference for the Sun Azimuth is the north marked with 0°, east corresponds to 90° and west to 270°. In the plots of Fig. 4.4 the variation of the global broad band irradiance † with the solar coordinates is shown with the data grouped by Clear Sky Index k^* ‡. In these plots the seasonal variations are also recognizable, especially in the plots including the solar azimuth angle. It is remarkable that for winter and autumn like conditions the increase of global broad band irradiance is steeper than in summer for clear sky conditions. This is related to the fact that during summer the turbidity of the atmosphere is in general higher than in winter.

4.2 Average-Photon Energy *APE*

APE is defined as the ratio of the broad band irradiance in a wavelength interval to the photon flux over the same interval, as it can be seen in equation 4.2. In this equation G_λ is the spectral irradiance density function in $W/m^2 \times nm$ and ϕ_λ is the spectral photon-flux density function in $photons/m^2 \times s \times nm$. Note that the photon flux is dependent on the corresponding spectral irradiance

*Universal Time Coordinated. For Germany $UTC = CET - TimeZone - SummerTime$. *CET* is Central European Time, *TimeZone* is the Time Zone of the location ($+1h$) and *SummerTime* refers to the time advance used in summer time ($1h$ or $0h$).

†It is important to recall that all the irradiances referred in this document are on horizontal plane unless otherwise stated.

‡The k^* values were calculated from the Cloud Index n values provided by *SOLIS*. For more information on n and k^* see [6] and [12]

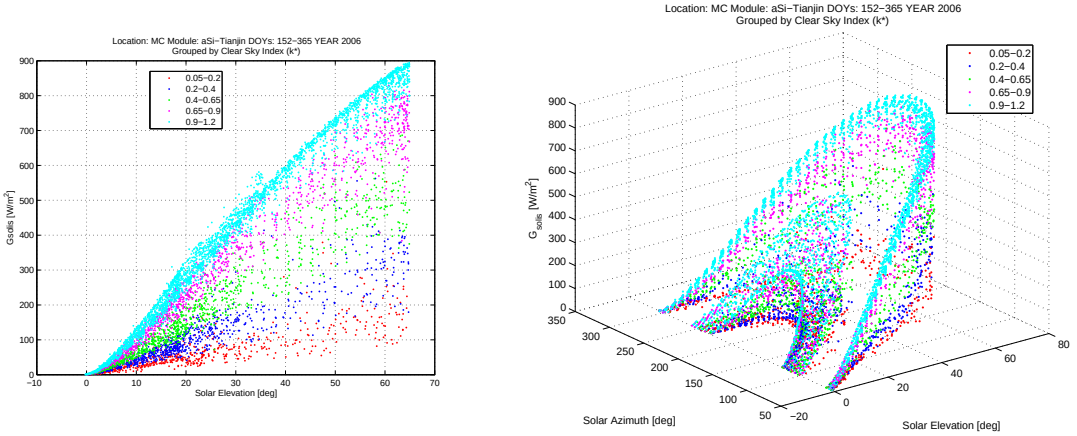

Figure 4.4: Global broad band irradiance dependence on Sun elevation (left) and Sun azimuth and Sun elevation (Right). The seasonal variations are better visualized in the last plot.

value and the photon energy at the given wavelength.

APE has units of energy (in this case Joules) and this is the energy of an average photon of a given spectrum in the wavelength window [a, b]. Given the order of magnitude of the *APE* values, a more appropriate unit to use is the Electronvolt. The value in *eV* is obtained from the one in Joules by dividing by the magnitude of the fundamental charge when expressed in Coulombs, $1.6e^{-19}$.

$$\begin{aligned} APE &= \frac{\int_a^b G_\lambda d\lambda}{\int_a^b \phi_\lambda d\lambda} \\ \phi &= \frac{G_\lambda}{hc/\lambda} \\ APE &= hc\frac{\int_a^b G_\lambda d\lambda}{\int_a^b \lambda G_\lambda d\lambda} \end{aligned} \tag{4.2}$$

APE is thought as a parameter for characterization of the solar spectra on Earth, without consideration of any properties of *PV* devices under investigation. Therefore it is cataloged as a *"device independent"* spectral parameter [§]. This should not be misunderstood: In practice the calculated

[§]In this chapter we will find plots of *APE* which are labeled with a given type of *PV* module. This is due to the fact that when calculating *APE* values other *device dependent* spectral parameters are also calculated.

APE values depend of course on the device or method used for obtention of the G_λ values.

Strictly speaking APE should always be calculated using the same integration limits a and b; however spectral irradiance measurement devices usually have different wavelength band-width and this results in different APE values for the same spectrum. In any case the band-width [a, b] must be wide enough and correctly positioned in the electromagnetic spectrum in order to include the major part of the extraterrestrial solar spectrum (a band from about 300nm to 2000nm minimum).

4.2.1 Calculation of *APE* with *SOLIS* Spectral Data.

For this work $SOLIS$ provide the satellite-based spectral irradiance data per band in W/m^2, i.e. the equivalent of the integrated spectral irradiance density over the given band. In this case the upper and lower integrals in equation 4.2 turns into simple sums. For the calculation of the photon fluxes per band we use the band spectral irradiance and the energy of a photon of the average wavelength of each band. In this way the discrete form of APE is:

$$APE = hc \frac{\sum_{i=1}^{N} G_{\lambda i}}{\sum_{i=1}^{N} \lambda_i G_{\lambda i}} \tag{4.3}$$

The APE values calculated from the *SOLIS* data use the 26 *SOLIS Kato-bands*, which cover the interval 306.8nm − 3001.9nm. The fact that the *Kato-bands* bandwidths are variable 5nm − 175nm, increases the uncertainty in the calculated APE value respect to cases which handle uniform bandwidths of 1nm or less. However the latest cases mean having much more data in regions where it is not quite meaningful.

The value of APE calculated for the spectrum of a black body at 5780K at the Earth-Sun distance using the *SOLIS Kato-bands* is 1.43eV. Other reference values for APE can be found in table 4.1 [2].

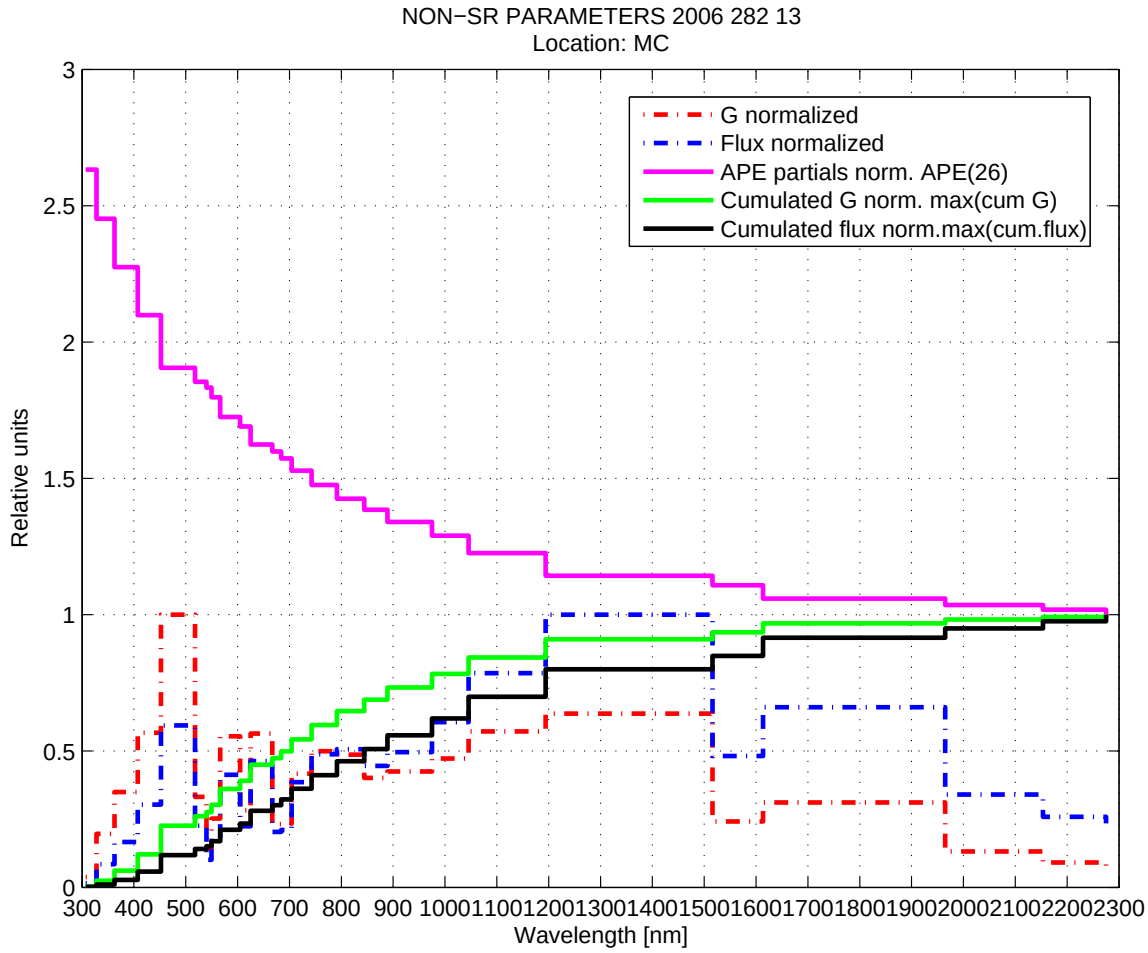

Figure 4.5: *APE* calculated up to the i^{th} band of *SOLIS*. The parameters used for its calculation are also shown. The data corresponds to the day of year (*DOY*) 282 of year 2006 at 13.186 hour. The shape of the spectral irradiance may look strange because the plotted values are the normalized values per *Kato-band* obtained directly from *SOLIS*.

Wavelength Range [nm]	APE [eV]
300-4000	1.43
300-2500	1.48
300-1700	1.62
300-1100	1.86

Table 4.1: Variation of the APE values calculated for the same AM 1.5G spectrum by integrating over different wavelength ranges, all of them starting in the UV region of the EM spectrum. [2].

4.2.2 Understanding APE

For a spectral parameter to be useful, it must describe changes in the chromatic content of the spectra. How does APE do it? The "*secret*" of APE lies in the fact that the energy of photons decreases with increasing wavelength. If we look at the mathematical form of APE in equation 4.2 and equation 4.3, we can see that the numerator and the denominator are accumulative terms which add sub-terms which can never be negative. In this way the only possibility for numerator and denominator is to increase over integration/sum.

Let's imagine that the spectral irradiance density is a constant over wavelength. In that case to obtain the same spectral irradiance at a higher wavelength requires higher photon fluxes. In this way as we integrate, the photon flux term in the denominator increases faster than the broad band irradiance term in the numerator does. Then we can see that APE values calculated up to a higher wavelength value for a given spectrum are lower than when integrating over a shorter λ range with the same starting point.

But this is a special case and certainly not what we encounter in the spectra of the sunlight on Earth, which are variations of a curved shape very similar to the one of a black body at $5780K$ (Planck's radiation law). Will our argument hold for this shape and for any other arbitrary shape of spectral irradiance density?

The answer is yes, we will get lower values of APE when integrating up to a higher wavelength. By observing the last expression in equation 4.2, we can see that:

1. The order of magnitude of the APE values is given mainly by the constant term hc, which is

5.2 Spectral Effects

At this point is necessary to realize that:

The plots of temperature-corrected specific short circuit current against global broad band irradiance should be equal to the plots of *Used Fraction* against irradiance. This holds when UD has been calculated with the actual spectral response of the *PV* device.

This is due to the equivalence of G_{ud} and I_{sc}. When using the relative spectral response the plots should differ in the values on the vertical axis but should keep the same proportions.

Before proceeding to compare these plots, we must perform the comparison of UD vs G and UD vs G_{solis}. For both devices they show that **relative to the measured irradiance, the *SOLIS* values are underestimated for cloudy conditions**. This is confirmed when we plot the *SOLIS* global irradiance against the measured irradiance (see Fig. B.2 on page 97). The Clear Sky Index values used for classification of the data into cloudy and no-cloudy conditions, were calculated from the satellite-measured Cloud Index. Therefore we can expect that this underestimation is due to errors in the calculation of the Cloud Index and the radiative transfer model (*RTM*) or only the first. Note that this underestimation of broad band irradiance may affect or not the calculated values of the spectral parameters UD and APE, depending on whether the underestimation is equally distributed in all *Kato- bands* (values are not affected) or not (values are affected). This underestimation is a first obstacle for distinguishing the spectral effects.

Now let's start the comparisons:

In Fig. 5.3 on page 63 we have the plots of Isc_{25}/G vs G for *a-Si* and *c-Si* and in Fig. B.3 on page 98 the plots of UD vs G (please keep in mind that the values of UD are calculated using the *SOLIS* spectral irradiance). The clearest fact is that the plots of specific short circuit current don't exhibit the stratification in k^* groups observed in the UD plots. For *c-Si*, after application of the Sun elevation filter, no fast decay of the values UD is seen for low irradiances; however a fast decay

of Isc_{25}/G can be appreciated. For *a-Si* the fast decay is observed in both type of plots. For the *c-Si* two different branches of Isc_{25}/G are recognized at low irradiances which I can not explain. Respect to the variations along the horizontal axis, the clear sky group is the only one which can be analyzed because it has a wide broad band irradiance range and the dispersion is not critical. From the plots of UD vs G and G_{solis} a slope[‡] of about $+10^{-5}m^2/W$ is calculated for *a-Si* and of $-10^{-5}m^2/W$ for *c-Si*. The calculation of the corresponding slopes in the plots I_{sc25}/G vs G give values of about $+10^{-7}m^2/W$ for both devices. It is interesting the change in sign of the slope for *c-Si*. This may be due to the uncorrected temperature effects. However a mismatch in the spectral responses may affect this trend also.

In Fig. 5.6 on page 67 we have the plots of Isc_{25}/G_{solis} vs G_{solis}. In this case the dispersion of the data for cloudy conditions is approximately 5 times bigger than in the case of measured irradiance. Despite of this fact one could say that the stratification of the k^* groups can be recognized at some extent, because for overcast situations there are very high values of I_{sc25}/G_{solis} which are clearly not superposed with any other k^* group. For the case of using *SOLIS* irradiance, the analysis of the slopes gives a positive slope for *a-Si* (about $10^{-7}m^2/W$). For *c-Si* the slope is nearly zero and difficult to determine whether positive or negative. In this case the changes in the slopes may be due also to mismatch of spectral response and uncorrected temperature effects, which for the *SOLIS* case are smaller.

In brief in none of the cases we can clearly observe the main spectral effect predicted with the plots $G_{udsolis}$ vs G_{solis}: the stratification of the k^* groups.

In another attempt to unmask the spectral effects, we can plot the specific short circuit current I_{sc25}/G and I_{sc25}/G_{solis} against the spectral parameters UD and APE. In the case of UD, what we ideally expect is to obtain a straight line with slope 1 and 0 intercept. Because we are using relative spectral responses, the slope should be dramatically reduced. In Fig. 5.7 on page 73 we see these plots, where no straight line can be clearly recognized due to high dispersion. In Fig. 5.8 bins of data have been made according to the Clear Sky Index groups. The order of magnitude of the values

[‡]an approximation calculated in the range $200W/m^2 - 800W/m^2$

in the vertical axis let us estimate the magnitude of the proportionality constant between the spectral response in A/W and the relative spectral response: $SR_{relative} \sim 10^2 SR$. Despite the binning, no trend can be defined due to the extreme dispersion and the tiny variations. However the binning suggests that for low UD values, dominated by clear sky conditions and temperatures above $25°C$, the values of I_{sc25}/G are overestimated. This may be due to the uncorrected temperature effects we see in Fig. 5.4 on page 65. In the case of I_{sc25}/G_{solis} increasing trends are outlined, and this suggests that indeed the overestimation of I_{sc25}/G for low APE values is due to temperature effects.

When plotting I_{sc25}/G and I_{sc25}/G_{solis} against APE the same trends are outlined. This can be seen in Fig. B.6 on page 101 and Fig. B.7 on page 102. In Fig. 5.9 on page 75 we see the dependence of UD on APE and we understand why the trends are kept. It is remarkable also, that in comparison to the same plots in chapter 4 (Fig. 4.12 on page 43), the *comet tails* for APE values under about $1.45eV$ are gone. This is a clear effect of the filtering of the data under 5° Sun elevation used for the I_{sc} model analysis.

Assuming a good correspondence between the satellite based k^* values and the ground measurements, the plots of temperature corrected short circuit current against measured irradiance grouped by k^* value (see Fig. 5.2 on page 62) should display the spectral effects clearly, which is not the case. Then how high should be the precision of the short circuit current measurements so that we are able to distinguish the spectral effects? According to the results of table 4.8 on page 55, for *a-Si* we expect 12% increase in I_{sc} values at fixed irradiance when the conditions turn from clear sky to overcast. For *a-Si* 8%. However for the site of measurements we have both cloud conditions at maximum $200W/m^2$. At this irradiance we have electric currents of about $0.5A$ for *a-Si* and $1.5A$ for *c-Si*. This means the minimum required precision for detecting the biggest spectral variations are about $0.05A$ and $0.15A$ respectively, which shouldn't be a problem for a decent measurement. However this is rarely the case, usually we have extreme cloud conditions at lower irradiances. At $100W/m^2$ the precision required would be $0.02A$ for *a-Si* and $0.08A$ for *c-Si*; at $50W/m^2$ $0.01A$ and $0.04A$ and so on. For the smallest variations (in terms of k^* groups), the required precision would be about 4 times higher; i.e. about $0.003A$ and $0.01A$ at $50W/m^2$. Besides there are precision require-

	***a-Si*: $I_{sc25} = (a \times G + b)$ Groups k^***				***a-Si*: $I_{sc25} = (a \times G_{solis} + b)$ Groups k^***			
$< k^* >$	a	b	R^2	$RMS\,E$	a	b	R^2	$RMS\,E$
[1]	$[A/(W/m^2)]$	$[A]$	[1]	$[A]$	$[A/(W/m^2)]$	$[A]$	[1]	$[A]$
0.11	0.0023	-0.020	0.976	0.031	0.002	+0.06	0.42	0.15
0.31	0.0021	-0.001	0.998	0.012	0.002	+0.00	0.70	0.13
0.51	0.0021	-0.007	0.993	0.034	0.002	+0.03	0.71	0.22
0.79	0.0022	-0.008	0.994	0.041	0.002	-0.09	0.83	0.22
1.00	0.0022	-0.032	0.998	0.025	0.002	-0.09	0.92	0.16

Table 5.1: *a-Si*: Fit parameters of temperature-*corrected* short circuit current against global broad band irradiance, fitting separately Clear Sky Index groups. The variation of the slope a gives the variation of the temperature-*corrected* short circuit current values due to spectral effects associated with clouds. Left: Using measured irradiance. Right: Using *SOLIS* irradiance.

	***c-Si*: $I_{sc25} = (a \times G + b)$ Groups k^***				***c-Si*: $I_{sc25} = (a \times G_{solis} + b)$ Groups k^***			
$< k^* >$	a	b	R^2	$RMS\,E$	a	b	R^2	$RMS\,E$
[1]	$[A/(W/m^2)]$	$[A]$	[1]	$[A]$	$[A/(W/m^2)]$	$[A]$	[1]	$[A]$
0.11	0.0080	-0.043	0.999	0.015	0.008	+0.24	0.49	0.49
0.31	0.0086	-0.071	0.985	0.130	0.009	+0.04	0.67	0.62
0.51	0.0081	-0.034	0.999	0.052	0.008	+0.22	0.67	0.91
0.79	0.0081	-0.038	0.998	0.110	0.009	-0.28	0.82	0.95
1.00	0.0081	-0.058	0.998	0.113	0.008	-0.19	0.93	0.64

Table 5.2: *c-Si*: Fit parameters of temperature-*corrected* short circuit current against global broad band irradiance, fitting separately Clear Sky Index groups. The variation of the slope a gives the variation of the temperature-*corrected* short circuit current values due to spectral effects associated with clouds. Left: Using measured irradiance. Right: Using *SOLIS* irradiance.

ments on the values of measured broad band irradiance. The bigger the uncertainty in the G values, the higher the required precision for I_{sc}. Because our estimations have been made on the basis of a 100% accurate G measurement, the I_{sc} measurements must be even more precise.

Because we measure broad band irradiance with a crystalline cell, we push even higher the precision standards for the I_{sc} measurements of *a-Si*. As we go down in irradiance values, the fluctuations in the electric current output of the devices are expected to increase, so we may find a point where no spectral effects can be recognized because of these random fluctuations due to the statistical nature of the interaction of irradiance with matter and the fact that we are measuring several cells which are in reality not identical.

In tables table 5.1 and table 5.2 on page 71 the results of the fits I_{sc25} vs G and I_{sc25} vs G_{solis} for k^* groups are shown [§]. The slopes of these fits should be proportional to the ones found in table 4.6 and table 4.7 on page 55. However in the new tables we can not recognize any trend or even significant change in the values of these slopes. This may suggest that the precision of our measurements is not sufficient. Nevertheless a mismatch of the spectral responses (actual and used for UD calculation) and non-corrected temperature effects may account for these observations. Because we did not estimate the uncertainties in the measured I_{sc} and G values, we cannot say whether the measurement precision may mask completely the spectral effects. This cannot be overlooked in future work. However we know that the uncertainties in the I_{sc} and G values depend not only in the precision of he measurements but also on the error introduced by the interpolation of the data.

INNER SUMMARY:

Up to now the results of this section confirm that we cannot recognize clearly the spectral effects:

1. Stratification of Clear Sky Index groups is not observed, not in the $I_{sc25}/G_{(solis)}$ vs $G_{(solis)}$ nor in the $I_{sc25}/G_{(solis)}$ vs UD or APE plots. In the first type of plots the great increase in the dispersion of the variable $I_{sc25}/G_{(solis)}$ for low irradiances overlap all the k^* groups . The

[§]Note that these statistical results are not the ones used for the evaluation of the quality of the models *G with k∗* and G_{solis} *with k∗*. The evaluation of the models is performed using the complete set of data, no matter if the fitting was done by groups or not.

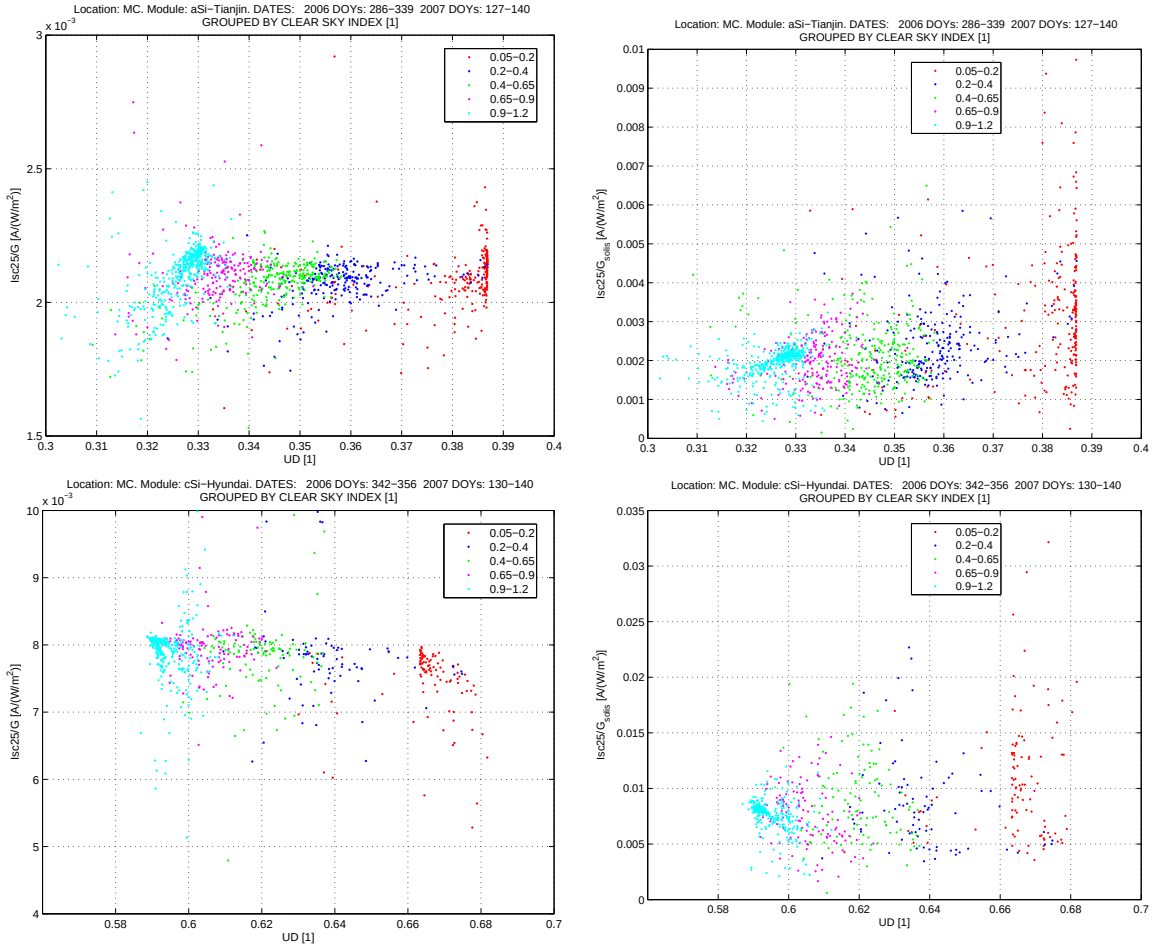

Figure 5.7: I_{sc25}/G and I_{sc25}/G_{solis} vs UD.

dispersion is also due to spectral variations related to Sun elevation variations. In the second type of plots the increased dispersion is distributed along the entire x-axis (UD or APE) and the uncorrected temperature effects are mostly present at low values of the spectral parameters (clear sky conditions). In these plots the data points in the upper part, which clearly define a limit line correspond to the data points with the highest irradiance values of each of the k^* groups.

2. The more subtle spectral effects related to Sun elevation variations are even more difficult to isolate because of the correlation between Sun elevation and module temperature together

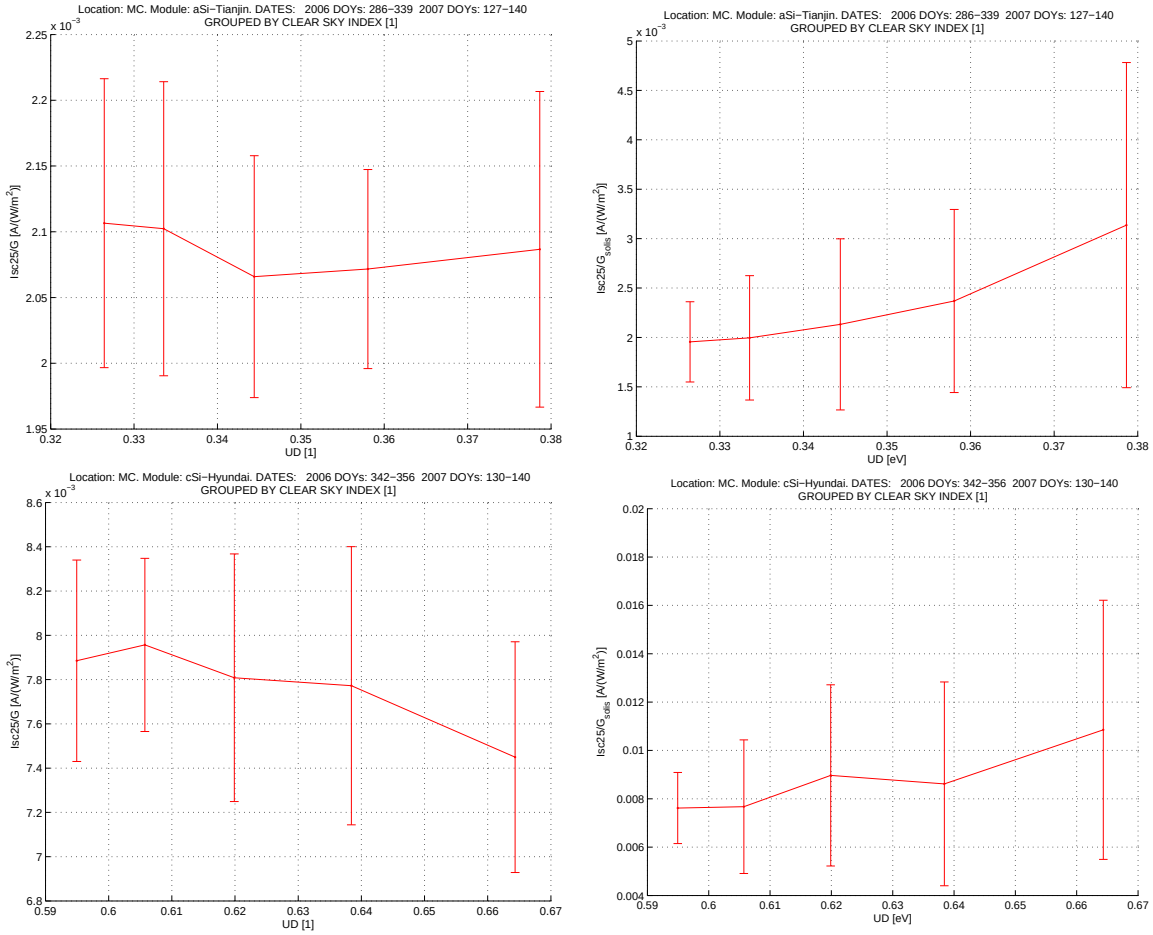

Figure 5.8: I_{sc25}/G and I_{sc25}/G_{solis} vs UD. Bins of data have been made according to the Clear Sky Index groups. The error bars correspond to the standard deviation of the bin.

with uncorrected temperature effects at high temperatures and irradiances.

END OF INNER SUMMARY

Now we will try to find factors which may account for the fact that we are unable to observe spectral effects. Because we have already discussed the influence of uncertainty in measurements, we will focus on other or related causes.

In Fig. 5.10 on page 76 the plots of temperature corrected short circuit current (I_{sc25}) against G_{ud} and $G_{udsolis}$ are presented. According to our discussion about the *Used Fraction* parameter UD, we

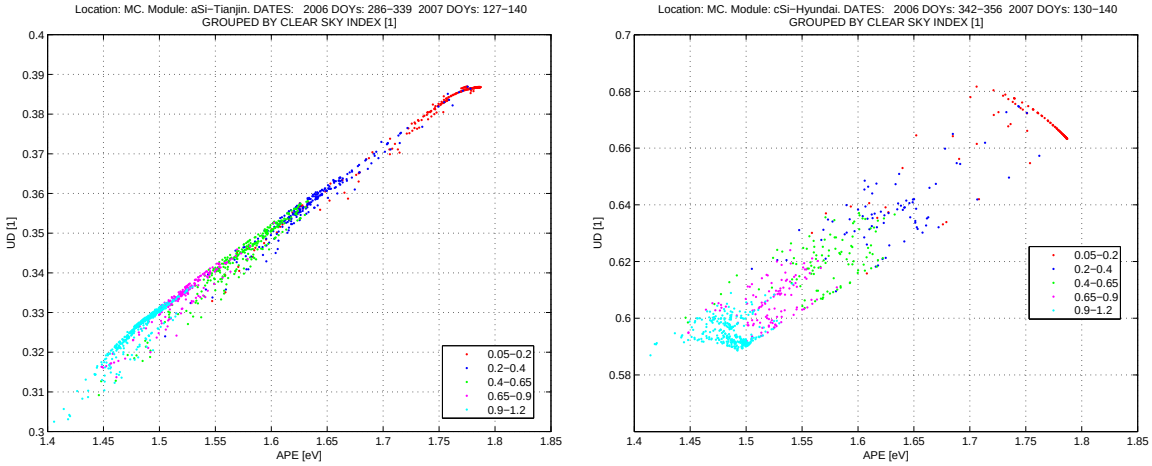

Figure 5.9: UD vs APE for the data used in the I_{sc} model analysis. Left: *a-Si*. Right: *c-Si*. Differences with the plots in Fig. 4.12 on page 43 are mainly due to the filtering of data under 5° Sun elevation.

expect to obtain a single straight line in each of these plots. Clearly our expectation is not fulfilled; however the splitting in the results is again magnified by the use of relative spectral responses with values between 0 and 1. In order to gain understanding we have to start by analyzing separately the cases of G_{ud} and $G_{udsolis}$.

In the case of G_{ud} the short circuit current values for cloudy conditions are under the values for clearer conditions for a fixed G_{ud} value. This is interpreted as an overestimation of the values of G_{ud} for cloudy conditions. Most probably this overestimation arises in the UD value than in the G value. On the side of G we could have non-corrected temperature effects. Nevertheless these effects are present most notably at high irradiances and high temperatures. So it looks like the UD values are overestimated for cloudy conditions. This can have 2 different reasons:

1. Arise directly from mismatching of the actual spectral response of the PV device and the spectral response used for UD calculations.

2. It may be related to the systematic underestimation of *SOLIS* broad band irradiance for cloudy conditions. As stated before, this underestimation may affect the values of UD if this phenomenon is caused by a systematic error in the calculation of the cloud index n: An erroneous

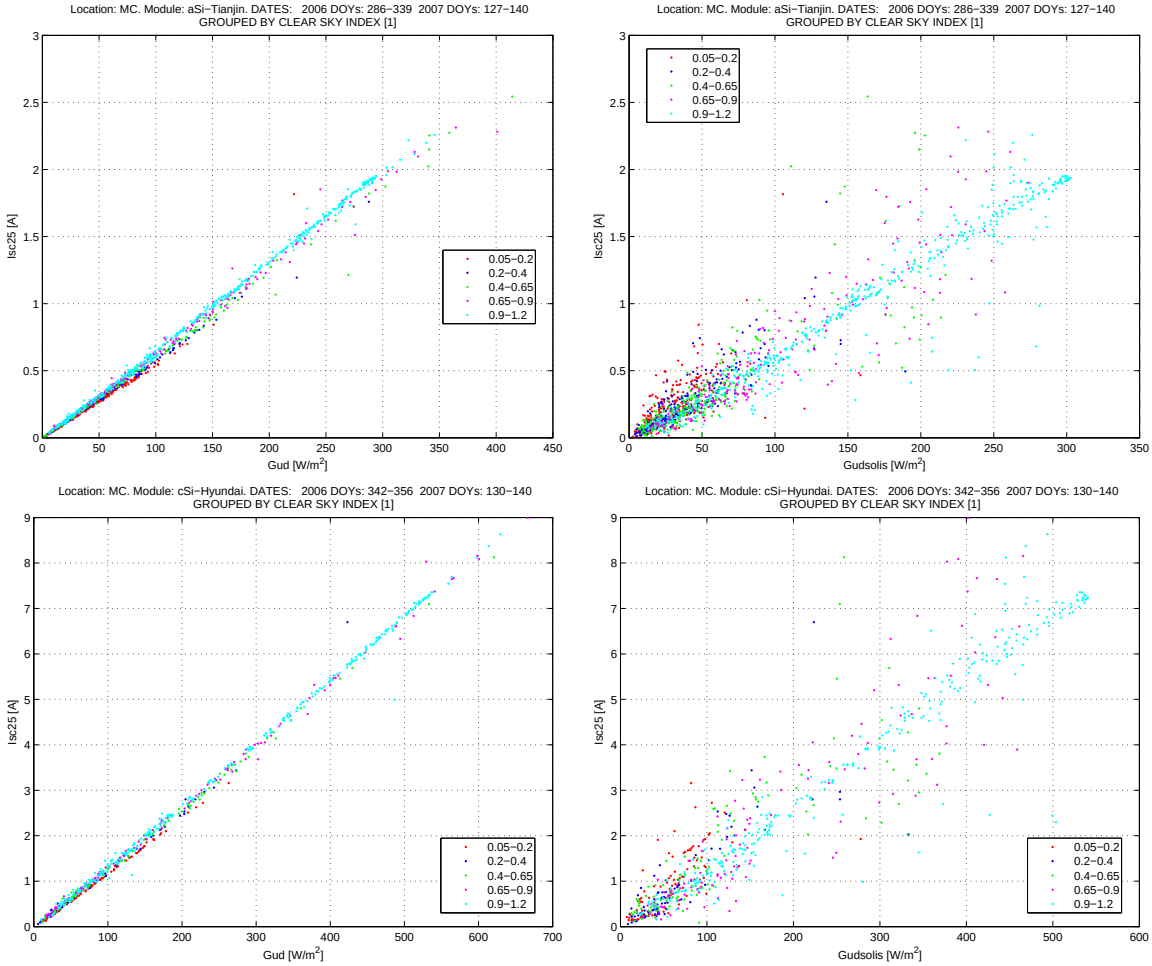

Figure 5.10: I_{sc25} vs G_{ud} and $G_{udsolis}$. Top: *a-Si*. Bottom: *c-Si*.

n value results in in a wrong *SOLIS* spectral distribution and therefore in a wrong UD value. So it may happen that too high values of *n* are calculated for cloudy conditions and therefore higher UD values are obtained. However I can not assure that the reductions in the *SOLIS* broad band irradiance values are always associated with an increase or even a change in UD.

In the case of $G_{udsolis}$ despite the high dispersion, the contrary effect can be distinguished although only for extreme cloud conditions : Under overcast conditions higher values of short circuit current are obtained that under clear sky conditions for a fixed $G_{udsolis}$ value. This is interpreted as underestimation of $G_{udsolis}$ values for cloudy conditions. How is this understood? The underestimation of

G_{solis} respect G is a fact and the measured G is expected to be better correlated to the short circuit current measurements. Moreover the previous case strongly suggests that an erroneous increase in the UD values is got for cloudy conditions. In this way the underestimation of the $G_{udsolis}$ values is the result of the superposition of the underestimation of G_{solis} and the overestimation of UD. This suggests that the overestimation of UD is minor compared to the underestimation of G_{solis} under cloudy conditions.

This hypothesis is reasserted by the plots of Fig. B.4 on page 99. In these plots we see that the cases G_{ud} vs G and $G_{udsolis}$ vs G_{solis} are consistent and in accordance with our expectations. Differently, the case $G_{udsolis}$ vs G is not what we expect. The first case is still consistent with our expectations despite it makes use of the *SOLIS* spectral data for the UD calculations. However the third cases collapses when we mix *SOLIS* broad band irradiance values with the corresponding measured values. Therefore this is the case we expect to find when modeling measured I_{sc} with pure *SOLIS* modified irradiance.

In any case it must be deeper investigated what are the reasons for the underestimation of the *SOLIS* broad band irradiance values for cloudy situations; with special attention on how the *SOLIS* spectral irradiance results affected.

5.3 Application of the I_{sc} Spectral Models

In this section the term I_{scca} is used. It stands for *calculated short circuit current* and refers to the modeled values which are finally used for the statistical analysis. These values are obtained after application of the temperature and the spectral models in the following order:

1. **Temperature Model:** For calculation of the I_{sc25} values.

2. **Spectral Model:** Calculates the values of temperature *corrected* short circuit current accounting for spectral effects (I_{sc25ca}).

3. **Temperature Model:** For going *back* from the modeled - temperature *corrected* values to the modeled values at the original temperature values (I_{scca}). These values are compared with the measurements.

In this way the chain of short circuit current values looks like this:

$$I_{sc} \rightarrow I_{sc25} \rightarrow I_{sc25ca} \rightarrow I_{scca}$$

Now we can proceed with the discussion about the application of the spectral models:

Despite we could not distinguish the spectral effects predicted with the *SOLIS* spectral irradiance data together with the relative spectral responses of the modules, we will apply the proposed models to observe what the results are. We expect that given clear spectral effects were not measured but only predicted, the models including UD and APE will collapse.

We have 10 models for each *PV* module. 5 correspond to the models which use ground measurements of global broad band irradiance and the other 5 to the ones using *SOLIS* broad band irradiance. From the 10 models 8 of them use information about the spectral composition of the light (by means of *SOLIS*-Satellite based k^* groups and /or the spectral parameters UD and APE) except the two reference models I_{sc} vs G and I_{sc} vs $Gsolis$.

The results for *a-Si* using measured irradiance are found in table 5.3 and in table 5.4 when using *SOLIS* irradiance. The corresponding results for *c-Si* are in table 5.5 and table 5.6 on page 80.

For the case of using measured broad band irradiance, all the models except one give the same results when we consider only the first significant figure in the statistical error parameters. The exception is the model I_{sc} vs G_{ud}, which gives worse results. It is surprising that the the models I_{sc} vs G_{ud} with k^* groups and I_{sc} vs $APExG$ with k^* groups don't collapse. This occurs because the non-existent spectral variations in I_{sc} introduced by the parameters UD and APE are clearly grouped in k^* groups (see Fig. 5.11); therefore fitting each group separately is consistent. This suggests that indeed no spectral effects can be resolved with precision of the measurements of I_{sc} and G and the

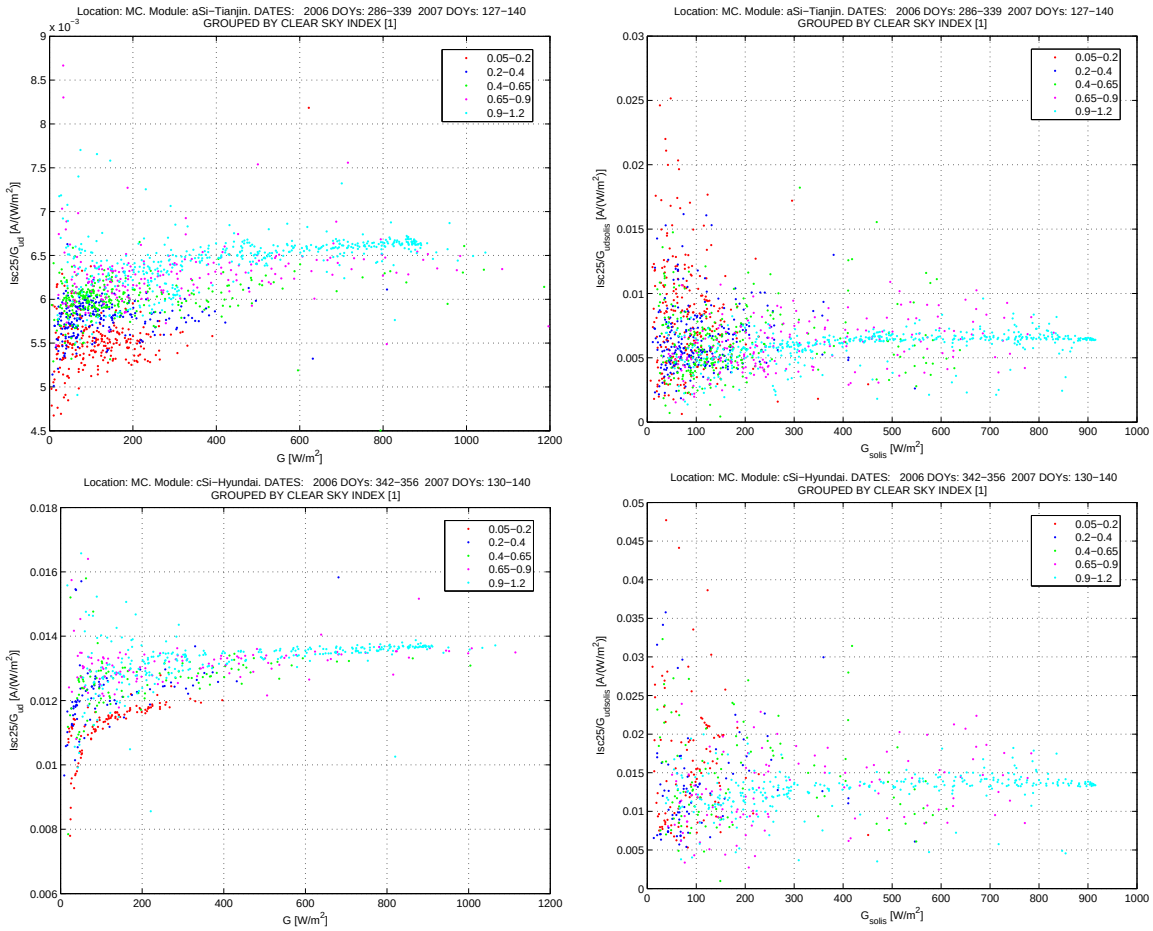

Figure 5.11: I_{sc25}/G_{ud} vs G and $I_{sc25}/G_{udsolis}$ vs G_{solis}. Top: *a-Si*. Bottom: *c-Si*. Because no spectral effects were found in the measured data, the use of G_{ud}, which assumes their existence, introduce artificial spectral dependencies. This is patent when measured broad band irradiance is used. For the case of *SOLIS* irradiance the high dispersion of the data masks these artificial variations (compare with plots of I_{sc25}/G_{solis} vs G_{solis} in Fig. 5.6 on page 67).

***a-Si*. BASED ON MEASURED IRRADIANCE** $< I_{sc} >= 0.571A$					
Model	$< I_{scca} >$ $[A]$	$Bias$ $[A]$	$Std.Error$ $[A]$	$RMSE$ $[A]$	$RMSE$ %
G	0.571	0	0.031	0.031	5.4
G_{ud}	0.571	0	0.040	0.040	7.0
G with k^*	0.571	0	0.029	0.029	5.1
G_{ud} *with* k^*	0.571	0	0.031	0.031	5.4
APExG with k^*	0.571	0	0.030	0.030	5.3

Table 5.3: Goodness of the fits for all the models used for I_{sc} for *a-Si*, using the ground measured values of broad band irradiance.

***a-Si*. BASED ON *SOLIS* IRRADIANCE** $< I_{sc} >= 0.57A$					
Model	$< I_{scca} >$ $[A]$	$Bias$ $[A]$	$Std.Error$ $[A]$	$RMSE$ $[A]$	$RMSE$ %
G	0.57	0	0.19	0.19	33.0
G_{ud}	0.57	0	0.18	0.18	31.5
G with k^*	0.57	0	0.18	0.18	31.5
G_{ud} *with* k^*	0.57	0	0.18	0.18	31.5
APExG with k^*	0.57	0	0.18	0.18	31.5

Table 5.4: Goodness of the fits for all the models used for I_{sc} for *a-Si*, using the *SOLIS* values of broad band irradiance.

***c-Si*. BASED ON MEASURED IRRADIANCE** $< I_{sc} >= 2.47A$					
Model	$< I_{scca} >$ $[A]$	$Bias$ $[A]$	$Std.Error$ $[A]$	$RMSE$ $[A]$	$RMSE$ %
G	2.47	0	0.10	0.10	4.0
G_{ud}	2.47	0	0.12	0.12	4.9
G with k^*	2.47	0	0.10	0.10	4.0
G_{ud} *with* k^*	2.47	0	0.10	0.10	4.0
APExG with k^*	2.47	0	0.10	0.10	4.0

Table 5.5: Goodness of the fits for all the models used for I_{sc} for *a-Si*, using the ground measured values of broad band irradiance.

***c-Si*. BASED ON *SOLIS* IRRADIANCE** $< I_{sc} >= 2.47A$					
Model	$< I_{scca} >$ $[A]$	$Bias$ $[A]$	$Std.Error$ $[A]$	$RMSE$ $[A]$	$RMSE$ %
G	2.47	0	0.74	0.74	30.0
G_{ud}	2.47	0	0.74	0.74	30.0
G with k^*	2.47	0	0.72	0.72	29.1
G_{ud} *with* k^*	2.47	0	0.72	0.72	29.1
APExG with k^*	2.47	0	0.72	0.72	29.1

Table 5.6: Goodness of the fits for all the models used for I_{sc} for *c-Si*, using the *SOLIS* values of broad band irradiance.

calculations based on *SOLIS* spectral irradiance; not even for *a-Si*. The relative statistical error is about 5.2% for *a-Si* and 4% for *c-Si*, however the absolute error is 3.3 times bigger for *c-Si* (due to the considerably smaller data set used for this module).

For the case of the models using *SOLIS irradiance* all the models, with no exception give the same results up to the first significant digit of *RMSE*, including the model I_{sc} vs G_{ud} with single fit. This shows that the non-existent variations introduced by the UD are insignificant in comparison to the huge data dispersion got when plotting measured short circuit current against a spectral parameter including *SOLIS* broad band irradiance.p to the first significant digit, the relative *RMSE* is 33% for *a-Si* and 28% for *a-Si*. The absolute *RMSE* for *c-Si* i 3.5 times the value for *a-Si*.